Live-cell imaging of dendritic spines by STED microscopy

U. Valentin Nägerl, Katrin Willig, Birka Hein, Stefan W. Hell, Tobias Bonhoeffer

Angaben zur Veröffentlichung / Publication details:

Nägerl, U. Valentin, Katrin Willig, Birka Hein, Stefan W. Hell, and Tobias Bonhoeffer. 2008. "Live-cell imaging of dendritic spines by STED microscopy." *Proceedings of the National Academy of Sciences* 105 (48): 18982–87. https://doi.org/10.1073/pnas.0810028105.

Live-cell imaging of dendritic spines by STED microscopy

U. Valentin Nägerl[a,1,2], Katrin I. Willig[b,1], Birka Hein[b], Stefan W. Hell[b,3], and Tobias Bonhoeffer[a,3]

[a]Department of Cellular and Systems Neurobiology, Max Planck Institute of Neurobiology, 82152 Martinsried, Germany; and [b]Department of NanoBiophotonics, Max Planck Institute for Biophysical Chemistry, 37077 Göttingen, Germany

Time lapse fluorescence imaging has become one of the most important approaches in neurobiological research. In particular, both confocal and two-photon microscopy have been used to study activity-dependent changes in synaptic morphology. However, the diffraction-limited resolution of light microscopy is often inadequate, forcing researchers to complement the live cell imaging strategy by EM. Here, we report on the first use of a far-field optical technique with subdiffraction resolution to noninvasively image activity-dependent morphological plasticity of dendritic spines. Specifically we show that time lapse stimulated emission depletion imaging of dendritic spines of YFP-positive hippocampal neurons in organotypic slices outperforms confocal microscopy in revealing important structural details. The technique substantially improves the quantification of morphological parameters, such as the neck width and the curvature of the heads of spines, which are thought to play critical roles for the function and plasticity of synaptic connections.

Structural plasticity of synaptic connections is considered to be a key mechanism in the brain whereby neuronal circuits are refined or remodeled during development and by experience. In recent years, advances in labeling and imaging techniques, notably two-photon laser scanning microscopy (1) using GFP-transgenic animals, have enabled the study of activity-driven structural dynamics at the level of single, identified synapses (2). For instance, it was shown that spines, which are the dendritic protrusions that form the postsynaptic part of most excitatory synapses in the mammalian brain, display a remarkable degree of structural plasticity, which is closely linked to functional changes in the strength of synaptic transmission, such as long-term potentiation (LTP) and long-term depression (LTD) (3–10).

Spines vary from 0.2 to 2 μm in length as measured by electron microscopy (11) and can thus be readily identified by confocal laser-scanning fluorescence microscopy. However, measuring changes in the shape and size of spines has been difficult because they are usually smaller than what conventional optical systems can reliably resolve. In practice, the lateral resolution of a standard two-photon microscope is >250 nm, while it is >200 nm for a confocal system. These resolving powers are insufficient for imaging finer details, such as the width of spine necks, which vary between 40 to 500 nm for spines on CA1 pyramidal neurons (11).

While changes in volume for structures that are below the diffraction limit can be estimated indirectly from changes in calibrated fluorescence intensities, as was recently performed for dendritic spines (5, 9, 10, 12), it is virtually impossible to visualize changes in shape of structures if they are below the resolution of the optical system. Given the critical role that the size and shape of synaptic structures is thought to play for synaptic function, it is important to measure their dimensions directly and faithfully in a living neuron.

Unlike confocal or two-photon microscopy, stimulated emission depletion (STED) microscopy (13) is not fundamentally limited by diffraction. A typical STED microscope uses a co-aligned scanning pair of focused laser beams, one for excitation and a doughnut-shaped one for STED, i.e., for de-exciting potentially excited molecules by stimulated emission. The resolution is largely given by $\Delta r \approx \lambda/(2NA\sqrt{1 + I/I_s}$ with NA denoting the numerical aperture of the lens, λ the wavelength and I the intensity at the crest of the doughnut-shaped STED beam. I_s is the intensity that is required for a (regularly focused) STED beam to cut down the fluorescence probability of the molecule by half (14–16); I_s is of the order of 10 MW/cm^2. STED microscopy has been used to study distributions of fluorescent antibody labeled proteins in fixed tissue preparations (14–16) and also to monitor movements of fluorescently labeled vesicles inside living nerve terminals (17). Recently, it was also applied to imaging the endoplasmatic reticulum of living PtK cells (18). Here, we demonstrate the power of this superresolution technique to image dendritic spines of YFP-positive CA1 pyramidal neurons in living organotypic hippocampal slices. Fine details such as the shape of the spine head or the width of the spine neck can be faithfully resolved and measured, even well below the surface of the tissue. Since it is suited for imaging living neurons, STED microscopy permits the imaging of activity-driven structural changes of spines with unprecedented clarity, revealing a diversity of shapes and dynamics that cannot be detected by established techniques.

Results and Discussion

We used organotypic hippocampal slices from YFP-transgenic animals, in which CA1 pyramidal neurons are strongly but sparsely labeled (19). Similar mouse lines have been previously used to study the activity-dependent regulation of the morphology of synaptic structures in time lapse experiments, typically relying on two-photon or confocal microscopy (6, 20, 21). Here, we used a custom-made stage-scanning STED microscope to image the dendritic structure of neurons in organotypic hippocampal slices maintained in a heated, artificial cerebrospinal fluid (ACSF)-containing recording chamber (Fig. 1*A*).

Confocal Versus STED Imaging of Dendritic Spines. To be able to directly compare the performance of STED with confocal imaging, we acquired images of dendritic spines in both modes by switching the STED laser beam on or off in an alternating

Author contributions: U.V.N., K.I.W., S.W.H., and T.B. designed research; U.V.N. and K.I.W. performed research; B.H. contributed new reagents/analytic tools; U.V.N. and K.I.W. analyzed data; and U.V.N., K.I.W., S.W.H., and T.B. wrote the paper.

The authors declare no conflict of interest.

Freely available online through the PNAS open access option.

[1]U.V.N. and K.I.W. contributed equally to this work.

[2]To whom correspondence should be addressed. E-mail: naegerl@neuro.mpg.de.

[3]S.W.H. and T.B. contributed equally to this work.

This article contains supporting information online at www.pnas.org/cgi/content/full/0810028105/DCSupplemental.

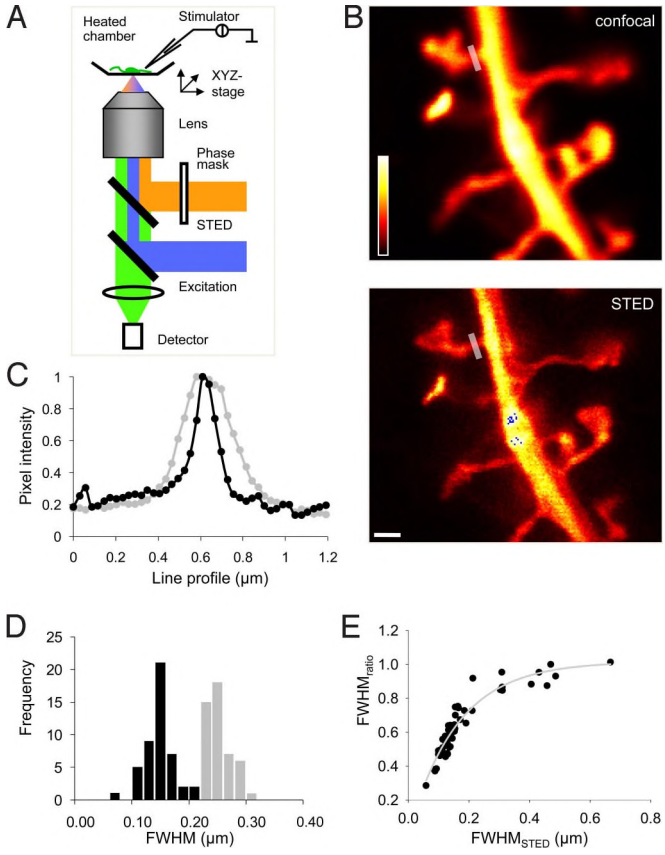

Fig. 1. STED microscopy of dendritic structures. (*A*) Schematic representation of the experimental setup. (*B*) Dendritic spines imaged either by confocal (*Top*) or STED (*Bottom*) microscopy. (Scale bar, 0.5 μm.) Note that pixel intensity representation is not saturated over the regions of interest, i.e., at the spine necks. (*C*) Normalized line profile of pixel intensity across the neck of a spine as imaged in confocal (gray curve) or STED mode (black curve); line width: four pixels, indicated by shaded bar in *B*. (*D*) Frequency histogram of FWHM values for spine necks imaged in confocal (gray bars) and STED (black bars) modes. (*E*) Plot of ratio of FWHM values in STED over confocal modes as a function of FWHM values of spine necks and dendritic shafts imaged in the STED mode.

fashion (Fig. 1*B*). The pulse peak intensity at the doughnut crest was $I = 400$ MW/cm^2, which in the case of negligible aberrations yields a focal plane resolution of $\Delta r \approx 69$ nm. From electron microscopy studies, it is known that spine necks, which are the elongated structures that connect the heads of spines with their parent dendrite, are among the smallest structures enclosed by the plasmalemma of neurons. As a consequence, many spine necks are beyond the limit of what conventional light microscopy is capable of reproducing in detail.

To assess how faithfully each mode can measure the size of the diameter of spine necks, we determined the full width at half maximum (FWHM) of line profiles of pixel intensities across the most narrow part of the spine necks. Fig. 1*C* shows that the normalized line profile for a typical spine is sharper in the STED than in the confocal mode, reflecting the fact that spine necks appear thinner in the STED than in the confocal images. We then plotted the FWHM values for a population of randomly selected spines, which were imaged in both modes (Fig. 1*D*). The frequency histogram shows that spine necks appeared consistently and significantly narrower when imaged in the STED as compared to the confocal mode ($FWHM_{STED} = 0.129 \pm 0.025$ μm vs. $FWHM_{confocal} = 0.233 \pm 0.022$ μm; mean $\pm$ SD; $n = 47$; $P < 10^{-30}$; paired t test). Importantly, the STED distribution (coefficient of variation [CV] = 0.195) is broader than the confocal distribution (coefficient of variation = 0.094), which is slightly skewed to the right. The CV is the ratio between the standard deviation and the mean, and represents a normalized measure of the dispersion of a probability distribution. Given that the standard deviation of the values for confocal and STED are comparable and that the mean STED value is about half the size of the confocal value, the CV is accordingly greater for STED than for the confocal mode. This is consistent with the view that the STED mode captures the variability of the diameters of the spine neck more faithfully than the confocal mode for which the lower values are tightly bound by the diffraction limit. Consistently, the mean $FWHM_{STED}$ value is about 70% larger than the mean of the three smallest values in the distribution (approximately 77 nm), while the mean $FWHM_{confocal}$ value is only by about 15% larger than the smallest values in the confocal distribution ($\approx$200 nm).

To assess the size of structures that can still be faithfully measured by confocal microscopy, we plotted the ratio (STED/confocal) of FWHMs measured in either mode against the width in the STED mode ($FWHM_{STED}$) (Fig. 1*E*) of a range of structures, including small ones such as spine necks and larger ones such as dendritic shaft diameters. The relationship is linear for small values of $FWHM_{STED}$ (<0.2 μm), while it asymptotes to unity for larger values (more than -0.3 μm), reflecting the fact that the FWHM values bottom out earlier for the confocal than the STED mode. This analysis confirms that the performance of the confocal mode is severely compromised for structures with sizes approaching its minimum focal spot FWHM of approximately 200 nm.

Compared to the conventional light microscopic pictures, the clarity of the images of the dendrite and the associated dendritic spines is significantly enhanced, revealing structural details reminiscent of volume reconstructions of electron microscopic serial sections. Fig. 2 shows two examples of volume rendered images of stretches of dendrite, based on a 3D image stack acquired by STED microscopy (also see supporting information (SI) Movie S1). Note that in these experiments, the axial resolution is that of a standard confocal system. However, recent advances show that the axial resolution can also be substantially improved by STED microscopy (22).

The images were acquired in the range of 0–10 μm above the surface of the coverslip without showing any decrease in resolution as might have been expected for STED imaging in optically dense tissue. The use of water objectives will help improve the depth penetration, given that oil objectives (as used in our experiments) produce more aberration because of the mismatch of refractive indices.

Time Lapse STED Imaging of Dendritic Spines. Next we examined whether this technique also lends itself to time lapse imaging. Since the peak intensity for STED ($I = 400$ MW/cm^2) is larger than the typical focal intensity of an excitation beam by about three orders of magnitude, we examined potential effects of phototoxicity and bleaching, which could make it impossible to acquire multiple time points. Fig. 3*A* illustrates that, at a practical level, neither phototoxicity nor bleaching associated with STED imaging were prohibitive. The panels show nine successive image frames of YFP-labeled dendrites out of a time lapse series of 20 image frames in total (see Movie S2), all of which were individually normalized to the respective peak value of pixel intensity. We extended the time lapse imaging to series up to 100 frames (data not shown), as well as to high-resolution 3D stacks (Fig. 2). These data demonstrate that the morphology of spines can be studied in time lapse experiments with a resolution <100 nm without compromising the integrity of the synaptic structures or the signal-to-noise ratio. This is not surprising given that (a) the STED beam intensity ($I = 400$ MW/cm^2) is much lower than

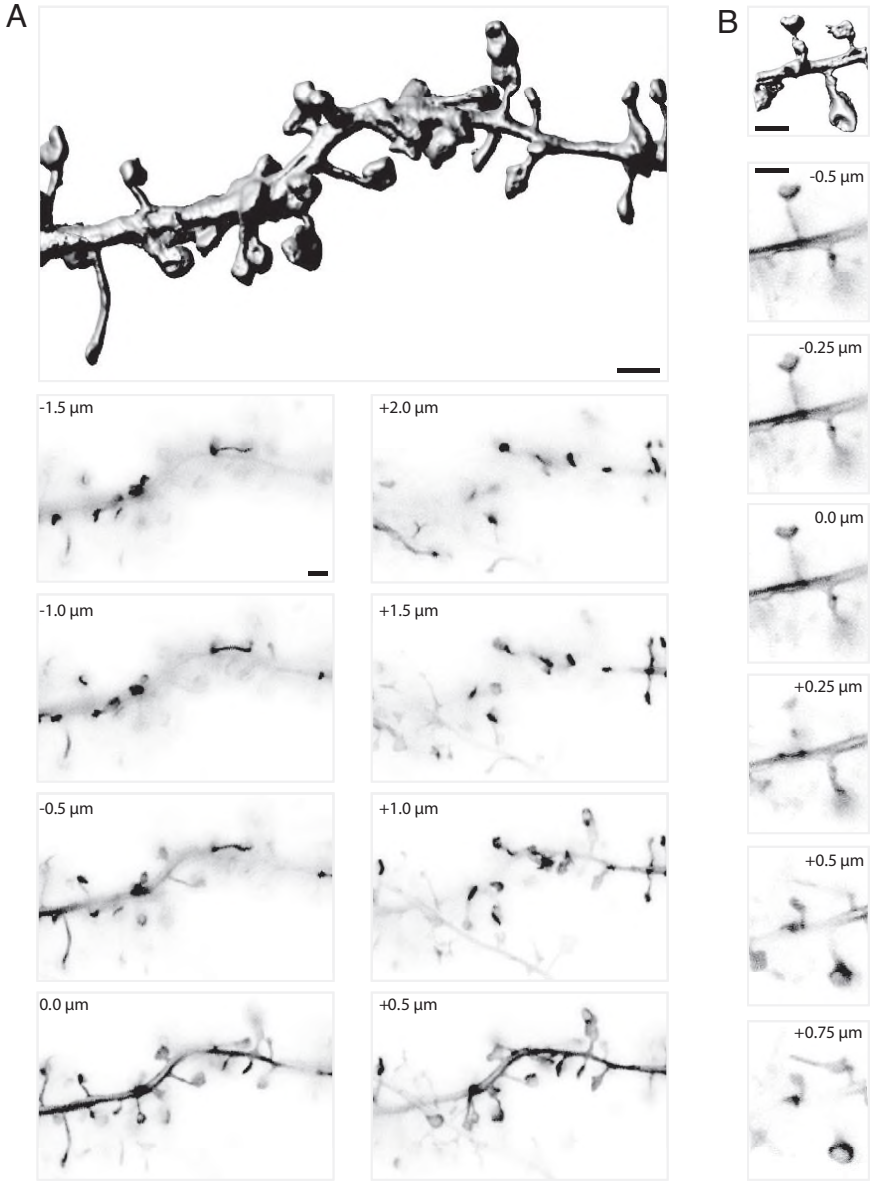

Fig. 2. High-resolution 3D STED imaging of dendritic structures. (*A*) Volume reconstruction of image stack data; the panels show individual image sections acquired at the z level indicated ($\Delta z = 0.5\ \mu m$). (*B*) Another example of a reconstructed stretch of dendrite ($\Delta z = 0.25\ \mu m$), the lateral pixel size was 29 nm/pixel in both cases. (Scale bars, 1 μm.)

intensity typically used for two-photon microscopy (200 GW/cm^2), and (b) that the absorption by water is much lower at the wavelength of 598 nm than in the near infrared range, resulting in negligible temperature rises in the focal region (<0.2K) (23).

To determine the degree of bleaching, we measured the pixel intensity averaged over the area of spine heads ($n = 14$ in total) and plotted this value over consecutive image frames acquired without interruption at 20 sec/frame (Fig. 3*C*). The graph illustrates that the pixel intensity decayed over the first few frames, before settling on a new level of around 50% of the initial value. This time course is consistent with the idea that the fraction of YFP that bleaches becomes replenished by diffusible YFP from areas within the dendrite that were not exposed to the beams. Therefore, one would expect the level of fluorescence to drop initially, converging on a steady-state value determined by the counteracting rates of bleaching and diffusion. Taken together, these data indicate that high-resolution STED microscopy is compatible with time lapse imaging, in particular if YFP is used as a volume marker. Our experiments indicate that STED imaging of neurons should work with any fluorescent indicator that is freely diffusible and which is quickly and continuously replenished after latent bleaching. This is likely to be the case for other genetically encoded indicators as well as small synthetic indicators such as Ca^{2+} sensitive dyes.

Imaging Activity-Dependent Structural Plasticity by STED Microscopy. Finally we used STED microscopy to image morphological plasticity of dendritic spines. To induce the structural changes we used the well-established synaptic plasticity paradigm of "chemical LTP," which involves raising neuronal activity in the entire slice by briefly perfusing it with a modified ACSF solution that globally potentiates synapses. Visual inspection showed that in the respective field of view, 40–60% of the spines changed shape after the stimulation (number of experiments = 4), while fewer than 10% of the spines appeared plastic under unstimulated conditions ($n = 5$). Alternatively, we used local tetanic stimu-

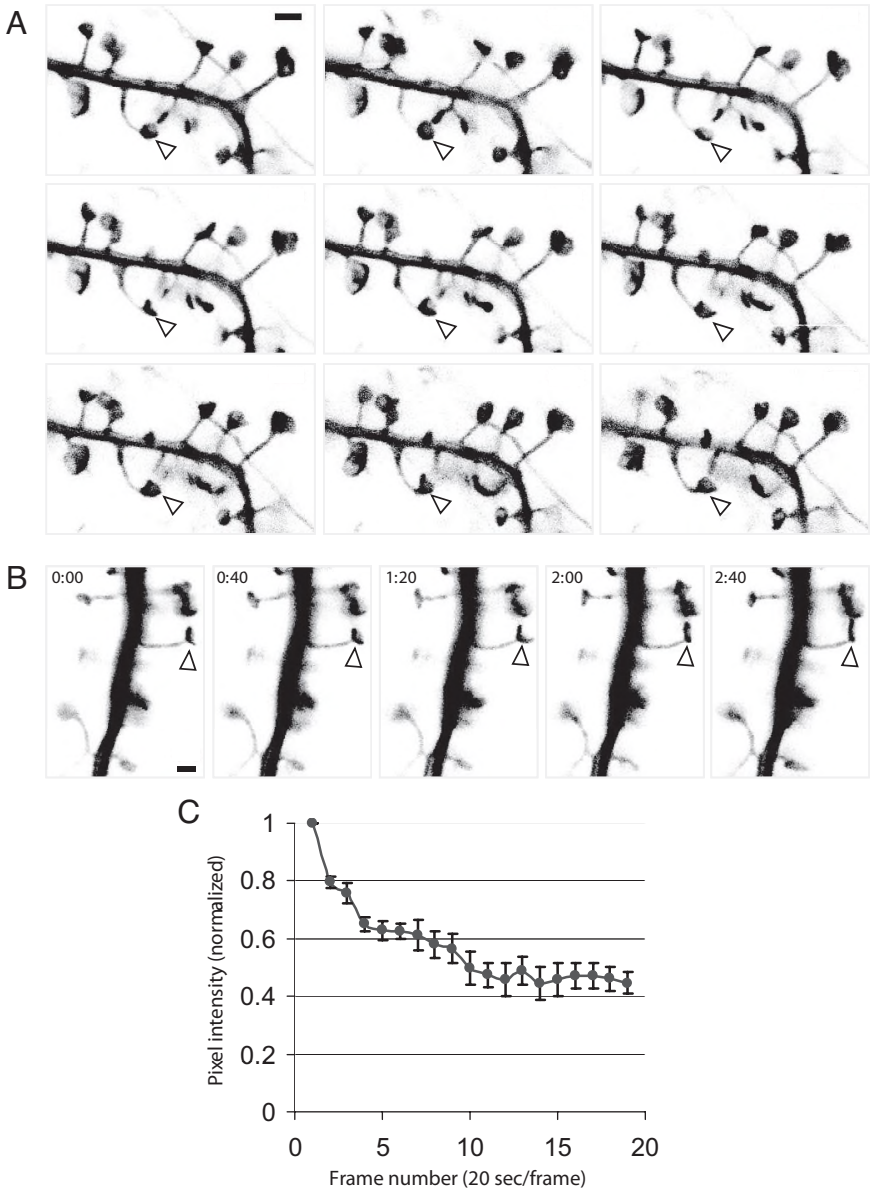

Fig. 3. Time lapse STED imaging of dendritic structures. (*A* and *B*) Series of image frames of YFP-labeled dendritic spines acquired by STED microscopy at 40 sec/frame (20 frames were acquired in total) under unstimulated conditions. Arrows indicate cup-like shapes of spine heads; STED pulse peak intensity 400 MW/cm^2 (*A*) and 215 MW/cm^2 (*B*). (Scale bars, 1 μm.) (*C*) Time course of fluorescence intensity in the heads of spines as a function of consecutively acquired image frames (20 sec/frame).

lation of afferent fibers projecting into the field of view which is a standard protocol for the induction of LTP in a synaptic pathway, which induced similar changes as the chemical LTP protocol (data not shown).

While it confirmed previous reports on activity-dependent size increases of dendritic spines (5), time lapse imaging using STED revealed details that are very difficult to detect by established light microscopy approaches, such as subtle changes in the shape of spine heads. In fact, due to the lack of resolution it had not been possible to examine structural changes other than simple changes in spine size. STED imaging now overcomes this limitation and permits studying the fine structure of spines in living tissue.

Fig. 4 illustrates the types of structural changes that can be observed by STED imaging. The images were acquired before (leftmost image) and after the plasticity-inducing stimulation at the times indicated. Fig. 4 shows examples of plastic spines, which change in size *and* shape considerably. Remarkably, the changes in shapes usually led from smaller and amorphous structures toward larger and more differentiated ones, often taking on cup-like shapes. For example, Fig. 4*C* shows a series of images of round spine heads morphing into cup-like structures. In addition, Fig. 4*D* shows a spine with a large head, which grows out before settling in a new position, where it changes shape from bulbous to cup-shaped. While some of these changes may represent instances of spine heads splitting into two parts, as reported by electron microscopy, others rather suggest a scenario whereby the spine changes shape after the plasticity-inducing stimulation to come into contact with its presumptive presynaptic partner.

These examples highlight the potential of STED microscopy for live cell imaging of genetically encoded fluorescence within the important neurobiological context of the structural plasticity of spines and synapses. STED microscopy may even make it

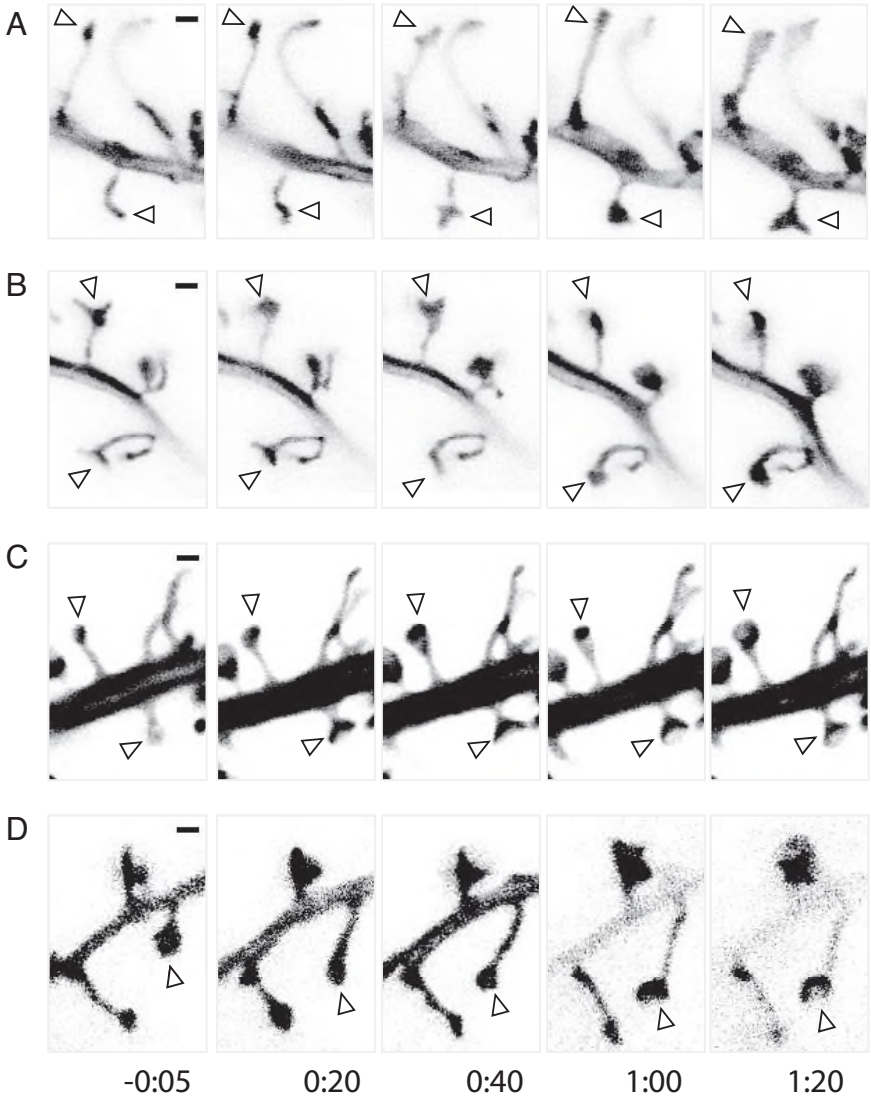

Fig. 4. STED imaging of activity-dependent postsynaptic morphological plasticity. (*A–D*) Examples of structural changes of dendritic spines after plasticity-inducing stimulation using the chemical LTP protocol. The first frame was taken before the stimulation, while all subsequent ones at the times indicated (h:min). Arrows indicate sites of structural rearrangements. (Scale bars, 0.5 μm.)

possible to assess functional synaptic connectivity simply from the synaptic morphology alone, replacing more complicated approaches such as correlative electron microscopy or functional labeling.

Experimental Procedures

Organotypic Hippocampal Slice Cultures. Hippocampal slices (300 μm thick) from postnatal day 5–7 wild-type C57/BL6J mice were prepared, embedded in a plasma clot on glass cover slips, and incubated up to two weeks in a roller incubator at 35 °C, according to the Gähwiler method (24). The age of the slice cultures for the experiments ranged between 14 to 21 days *in vitro* (DIV) after the preparation. For the experiments, cultures were transferred into a heated chamber (35 °C), where they were maintained in standard ACSF solution containing (in mM): NaCl 126, KCl 2.5, $CaCl_2$ 2.5, $MgCl_2$ 1, glucose 10, and Hepes 20. The pH was adjusted with NaOH to 7.3.

Plasticity-Inducing Stimulation. Slices were imaged over a baseline period (typically acquiring three time points) before they were subjected to two different experimental paradigms that are commonly used to induce functional and structural plasticity at hippocampal synapses. The ACSF designed to induce ''chemical LTP'' contained (in mM): NaCl 124, KCl 5, $MgCl_2$ 0.1, $CaCl_2$ 5, glucose 10, TEA 25, and Hepes 29, and its pH was adjusted to 7.3. This modified ACSF solution was washed in for a period of 5 min before it was washed out by the standard ACSF solution. In the experiments using electrical stimulation, brief (0.2 ms) current pulses (10 μA) at 100 Hz for 1 sec (repeated 5 times at 60 sec intervals) were delivered via a patch pipette positioned under visual control and with the help of a micromanipulator within 20 μm of the field of view that contained the dendrites that were imaged.

STED and Confocal Microscopy. We used excitation pulses of 100 ps and 490 nm that were synchronously followed by 300 ps STED pulses having a central wavelength of 598 nm. The 80MHz pulse trains were focused by a 1.4 NA objective lens (PL APO, 100×, oil, Leica). The excitation pulses were delivered by a pulsed laser diode (Toptica) at an average focal power of 1.7 μW. The fluorescence collected by the lens was separated by a dichroic mirror, filtered via a 525/60 bandpass and imaged onto a multimode optical fiber. The diameter of the fiber amounted to 80% of the back-projected Airy disk and therefore functioned as a confocal pinhole. The STED pulses originated from an optical parametric oscillator (OPO, APE) fed from a Ti:Sapphire laser (MaiTai, Spectra-Physics) operating at 800 nm. Originally of 200 fs duration, the OPO pulses were stretched by dispersion in a polarization preserving fiber (OZ Optics) of 120 m length to approximately 300 ps. The time-averaged power P_s of the STED beam reducing the fluorescence by half was identified in a separate measurement as 0.9 mW. The excitation pulses were synchronized with the STED pulses via external triggering of the laser diode; the delay was tuned using a home-built electronic delay generator. The expanded STED

beam passed through a polymeric phase plate imprinting on the wavefront a helical phase delay of exp($i\phi$), with $0 < \phi < 2\pi$ (RPC Photonics) which delivers a doughnut at the focal region of the lens. The count rate was compensated for the dead time of the avalanche photodiode (APD, SPCM-AQR-13, PerkinElmer) by multiplying the measured count rate with a correction factor of $1/(1-t_d*CR)$; t_d = 50 ns is the dead time of the APD and CR the measured count rate.

Image Acquisition and Analysis. Images were acquired with a pixel size of 29 nm over a field of view of up to 25 μm $\times$ 25 μm in size. At least one image frame was taken in the confocal mode before STED imaging began. Depending on the size of the field of view that was imaged, the frame rate was 20 or 40 sec/frame. Images or image stacks (Δz = 0.5 μm) were acquired repeatedly (typically 20 frames in a series, but up to 60) at variable time points (at the maximal frame rate or at 10 min intervals) without any signs of photo damage. The imaging depth typically varied between 0 and 10 μm below the surface of the cover slips.

Images were analyzed using ImageJ. Values of FWHM were extracted from line intensity profiles of the narrowest part of spine necks using a fitting routine written in Matlab (Mathworks). Statistical significance was tested using SigmaPlot 8.0 (SPSS Inc.). All images shown are raw, unprocessed images, except for the volume-rendered image stack in Fig. 1*B*, which was generated using Imaris (Bitplane AG).

1. Denk W, Strickler JH, Webb WW (1990) 2-Photon Laser Scanning Fluorescence Microscopy. *Science* 248:73–76.
2. Yuste R, Bonhoeffer T (2001) Morphological changes in dendritic spines associated with long-term synaptic plasticity. *Annu Rev Neurosci* 24:1071–1089.
3. Engert F, Bonhoeffer T (1999) Dendritic spine changes associated with hippocampal long-term synaptic plasticity. *Nature* 399:66–70.
4. Maletic-Savatic M, Malinow R, Svoboda K (1999) Rapid dendritic morphogenesis in CA1 hippocampal dendrites induced by synaptic activity. *Science* 283:1923–1927.
5. Matsuzaki M, Honkura N, Ellis-Davies GCR, Kasai H (2004) Structural basis of long-term potentiation in single dendritic spines. *Nature* 429:761–766.
6. Nägerl UV, Eberhorn N, Cambridge SB, Bonhoeffer T (2004) Bidirectional activity-dependent morphological plasticity in hippocampal neurons. *Neuron* 44:759–767.
7. Nägerl UV, Kostinger G, Anderson JC, Martin KAC, Bonhoeffer T (2007) Protracted synaptogenesis after activity-dependent spinogenesis in hippocampal neurons. *J Neurosci* 27:8149–8156.
8. Becker N, Wierenga CJ, Fonseca R, Bonhoeffer T, Nägerl UV (2008) LTD induction causes morphological changes of presynaptic boutons and reduces their contact with spines. *Neuron* 10.1016/j.neuron.2008.09.018.
9. Tanaka JI, *et al.* (2008) Protein synthesis and neurotrophin-dependent structural plasticity of single dendritic spines. *Science* 319:1683–1687.
10. Zhou Q, Homma KJ, Poo MM (2004) Shrinkage of dendritic spines associated with long-term depression of hippocampal synapses. *Neuron* 44:749–757.
11. Harris KM, Kater SB (1994) Dendritic Spines—Cellular specializations imparting both stability and flexibility to synaptic function. *Annu Rev Neurosci* 17:341–371.
12. Lang C, *et al.* (2004) Transient expansion of synaptically connected dendritic spines upon induction of hippocampal long-term potentiation. *Proc Natl Acad Sci USA* 101:16665–16670.
13. Hell SW, Wichmann J (1994) Breaking the diffraction resolution limit by stimulated-emission—stimulated-emission-depletion fluorescence microscopy. *Optics Letters* 19:780–782.
14. Kittel RJ, *et al.* (2006) Bruchpilot promotes active zone assembly, Ca2+ channel clustering, and vesicle release. *Science* 312:1051–1054.
15. Sieber JJ, Willig KI, Heintzmann R, Hell SW (2006) Lang T The SNARE motif is essential for the formation of syntaxin clusters in the plasma membrane. *Biophys J* 90:2843–2851.
16. Willig KI, Rizzoli SO, Westphal V, Jahn R, Hell SW (2006) STED microscopy reveals that synaptotagmin remains clustered after synaptic vesicle exocytosis. *Nature* 440:935–939.
17. Westphal, *et al.* (2008) Video-rate far-field optical nanoscopy dissects synaptic vesicle movement. *Science* 320(5873):246–249.
18. Hein B, Willig KI, Hell SW (2008) Stimulated emission depletion (STED) nanoscopy of a fluorescent protein-labeled organelle inside a living cell. *Proc Natl Acad Sci USA* 105:14271–14276.
19. Feng GP, *et al.* (2000) Imaging neuronal subsets in transgenic mice expressing multiple spectral variants of GFP. *Neuron* 28:41–51.
20. Holtmaat AJGD, *et al.* (2005) Transient and persistent dendritic spines in the neocortex in vivo. *Neuron* 45:279–291.
21. Trachtenberg JT, *et al.* (2002) Long-term in vivo imaging of experience-dependent synaptic plasticity in adult cortex. *Nature* 420:788–794.
22. Schmidt R, Wurm CA, Jakobs S, Engelhardt JEA, Hell SW (2008) Spherical nanosized focal spot unravels the interior of cells. *Nat Methods* 5:539–544.
23. Schonle A, Hell SW (1998) Heating by absorption in the focus of an objective lens. *Optics Letters* 23:325–327.
24. Gähwiler BH (1981) Organotypic monolayer cultures of nervous tissue. *J Neurosci Methods* 4:329–342.